Строительство уникальных зданий и сооружений. ISSN 2304-6295. 12 (27). 2014. 76-89

Construction
of Unique Buildings and Structures

journal homepage: www.unistroy.spb.ru

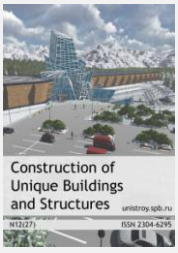

The connections between the displacements and the applied loads for reinforced-concretes plates

B. Kovacic[1], **R. Kamnik**[2]

University of Maribor, Smetanova ul. 17, SI – 2000, Maribor, Slovenia

ARTICLE INFO

Original research article

Article history

Received 22 December 2014
Accepted 28 December 2014

Key words

measurement of displacements,
electronic tacheometer,
photogrammetry,
pressure length transducer on the hydraulic cylinder,
reinforced-concrete plate

ABSTRACT

Nowadays, the method of displacement measurements on constructions is well known. A variety of equipment of different accuracy and capacity is available. In this paper authors present a combined method of tacheometric and photogrammetric measurements and displacements measured by a pressure length transducer. In our laboratory, the loading of the pre-stressed concrete plate occurred in steps of 3 kN. The Mathematica 5.0 program was used to calculate the interpolation polynomials. All results were compared to the calculated values (using in the Eurocode 2) with the help of interpolation polynomials. The results show that, in future, we will not need to use so many load phases, because the intermediate displacements can be calculated from the obtained equations and the displacements under different loads predicted.

Contents

[1] *Corresponding author:*
bostjan.kovacic@uni-mb.si (Bostjan Kovacic, Ph.D., Professor)
[2] rok.kamnik@um.si (Rok Kamnik, Ph.D., Associate Professor)

Introduction

The method of displacement measurements on constructions is well known. The decision on which method should be used depends on the size of the structure, its accessibility and the required accuracy. It is recommended to use two independent methods at the same time. This increases the costs and the measurement time, but it assures more accurate results if we keep in mind that geodetic methods cannot be repeated under the same conditions. For the load testing of structural elements, both geodetic and physical methods are used. So, at identical measurement points the vertical displacements as well as strength and inductivity changes are obtained with the help of strain gauges and inductive transducers or accelerometers. The results are a good indicator of the relationship between displacements and deformations. Total stations, photogrammetric instruments and different length transducers are used in our field work. To achieve the best possible results, our methods have to be compared to other ones. For this purpose a comparative analysis of the results, which were gained from measurements as well as from values of displacements, was carried out.

In our laboratory, the loading of the pre-stressed concrete plate occurred in steps of 3 kN. The Mathematica 5.0 program was used to calculate the interpolation polynomials.

First of all, the measurement of vertical displacements and deformations on structural elements is carried out during construction for control, after-construction for object monitoring and for reliability assessment after a certain time of usage [2]. Nowadays, more attention is paid to the maintenance of existing objects, so more and more research is required from laboratories. Because laboratories provide ideal meteorological conditions, which cannot be assured on the field, a high quality comparison and analysis can be achieved.

The most widely used as well as the fastest and the most accurate method are the trigonometric heighting method. The highest quality results are met if this method is combined with photogrammetry. So far, photogrammetric measurements were mostly used for the needs of architecture (facades), cultural heritage (archeological sites), medicine (face, body, skin, eye modelling) and industry (quality control). With the development of accuracte in digital photography [3] a precise monitoring of the deformations of objects of interest like concrete plates, bridges, buildings… is possible [4], [5]. Bellow, a short description of used methods is given. [1-20]

Trigonometric heighting method

Among the classical geodetic methods, the trigonometric heighting method was used. An electronic tacheometer (total station) (NIKON DTM 700 Series) was used to observe directly the height difference between two points, i.e. by measurement of the zenith angle and the slope distance, according to the general equation (1):

$$\Delta H = S \cdot \cos Z_A + i_A - l_B + \left(\frac{1-k_a}{2}\right) \cdot \left(\frac{S^2 \sin^2 Z_A}{R}\right) \quad (1)$$

where:

S – slope measured distance between *A* and *B*

Z_A – zenith angle

i_A – height of instrument at point A

l_B – height of prism at point B

k_a – coefficient of refraction (for lines high above the ground 0.13; in laboratory is 0.0; [6])

R – Earth radius as a sphere ($R = \sqrt{M \cdot N}$; M - radius of curvature along the meridian, N - radius of curvature in the prime vertical)

In Eq. (1) the height of instrument i_A can be omitted because the measurements were in a relative coordinate system and all measurement were of a fully local nature. The height of prisms in Eq. (1) can also be omitted, because the reflective tape targets, used for the marking of the measurement points, have no prism height as such and negligible thickness.

In consequence,

$$\Delta H = S \cdot \cos Z_A + \frac{S^2 \sin^2 Z_A}{2R} - k_a \frac{S^2 \sin^2 Z_A}{2R} \quad (2)$$

In the Eq. (2) the refraction coefficient can be taken as zero because of the laboratory conditions. So, the final equation is:

$$\Delta H = S \cdot \cos Z_A + \frac{S^2 \sin^2 Z_A}{2R} \quad (3)$$

Each point on the concrete plate was observed from one observing station (set up one day in advance). The measurements were made from a tripod that was glued to the ground to minimize shifts of the instrument. The post-processing of all recorded data was carried out before the analysis (filtering). In this way, all possible errors were eliminated, such as double observations of the same point, wrong order of sightings, etc. The observations of the zenith angles and slope distances were arranged according to individual epochs. Every epoch (of loading or unloading) was compared with the zero state, which was recorded at the start of the measurements by observing the control points on the wall of the laboratory.

After the measurement, the data were processed and analyzed. For every target, the standard deviation was calculated. In every measurement epoch, each point was measured ten times (slope distance, horizontal direction and zenith angle) in the precise measurement mode of the instrument (PMRS). The arithmetic mean value was calculated for all measured quantities [7]. The achieved precisions of measurements (mean of eight) are shown in Table 1.

Table 1. Standard deviation by observation type

Observation	Standard Deviation *s*
slope distance	0.16 mm
horizontal direction	3.0''
zenith angle	3.4''
Y	0.13 mm
X	0.13 mm
Z	0.11 mm

Photogrammetric method

Stereo-photogrammetry is an optical measuring method which has become a standard method in geodesy, civil engineering and architecture in past few decades. The measuring object was recorded using a stereo-photogrammetric system TRITOP with high resolution CCD camera Fuji Pro S3 (4256 x 2848 pixels). The computer processing of the stereo-images followed afterwards. The picture coordinates of the measuring points were determined with numerical procedures. The 3D object coordinates were then calculated using the principle of triangulation. This method is suitable for the accurate measurement of positions in space, three-dimensional displacements and, in the case of a large number of points, objects shape and deformation.

Generally, the picture coordinates (x, y) are a function of six parameters of the external orientation – projection center coordinates O (X_0, Y_0, Z_0) and rotation angles (ω, φ, κ) – and three parameters of the internal orientation – camera constant c and picture coordinates of the images principal point H (x_0, y_0). Thus, if the external and internal orientations of the camera are known we can calculate the picture coordinates x, y for every object point.

A problem appears if we want to calculate the object coordinates from the picture coordinates. The three unknown object coordinates X, Y, Z can only be calculated from two measured picture coordinates if we assume that we are observing a flat object which is perpendicular to recording direction so that the Z coordinate is constant and known for all measuring points. For measuring objects in space it is necessary to take at least one more image from an different angle so that for every measuring point three or more picture coordinates can be measured. For this purpose, the stereoscopic effect and the method of triangulation are being used. In our case eight pictures were taken for each loading epoch.

This principle has been used from the very beginning of stereo-photogrammetry when the measuring object was recorded with cameras from multiple positions after which the pictures (stereo pairs) were being processed with special devices called stereo comparators. The object (space) coordinates of the measuring points were determined directly using the so-called opto-mechanical reconstruction procedure.

In today's stereophotogrametric measurements, an automatic analytical procedure is being used. On the stereo pairs, which are recorded with CCD cameras, the picture coordinates of the measuring points are measured with software. For every picture coordinate one equation is formulated. Provided that the number of the measuring points (and, thus, the number of equations) is larger than the number of unknown camera parameters, the system of equation becomes over defined. Thus a solution needs to be found with a least square method.

In the classic stereophotogrammetry, the measuring points are defined with the help of known details on the measuring object or by measuring marks. If the measuring marks are recorded well, the accuracy of the method is very high. For measuring the position in space, movement tracking, and deflection measurement and in applications where high point density is not necessary, the stereophotogrammetric method is the most powerful among the optical methods. Photogrammetry is a versatile and efficient full field three-dimensional measurement technique, offering a high precision potential at reasonable cost [9].

Pressure transducer method

A hydraulic cylinder PZ10 (Telem d.o.o) was used. There were 14 epochs between which the load increased 3 kN at a time. Each epoch was held for 400 s (static load) so that the points could be observed and photographs could be taken. During the next 100 s, the hydraulic cylinder PZ10 increased the force by 3 kN. The vertical deformation of the central point of the concrete plate was measured with extensometer with a very precise measuring rod attached to the hydraulic cylinder. The rod has an electrical output (4 mA – 20 mA) by which the increment of vertical displacement was determined with accuracy of 5 □m. The cylinder was controlled by LabVIEW software.

Description of experiment

In order to compare the measurement methods described above, a prefabricated pre-stressed concrete plate, which is frequently used for industrial buildings, was tested (fig. 1). The decision for a laboratory (rather than field) experiment was made due to the constant conditions of loading flow and equal measurement results. The predicted vertical displacement was calculated using the static design with the vertical force in the middle of the span.

The object was monitored by 210 points (points on the structure and points on the walls of the laboratory for control) in a local (object) coordinate system. Each point was observed 10 times. Leica's reflective tape targets of dimensions 1 x 1 cm were used as points on the structure. In Fig. 2, the reflective tape targets 4, 5 and 6 in the middle of the concrete plate, where the breakage was expected, are shown. For the analysis, the points 4 and 6 were omitted.

Figure 1. Prefabricated prestressed concrete plate with measured marks

Code targets were glued in the proximity of the Leica targets for the comparison of the measurement methods (trigonometric heighting and stereo-photogrammetry) so that it was possible to compare the measured vertical displacements from both methods (figure 2). The center of the coded targets is a white circle of 18 mm diameter on the black background. The coded marks had a 15 byte type code (using circle sectors) to allow identification in every image. The correct distance between measuring points is determined with scale bars whose distance is known (in our case the distance between two code marks) and does not change during the measurement. After processing, the results gained with photogrammetric method can be shown in the form of vectors or color scale (figure 3).

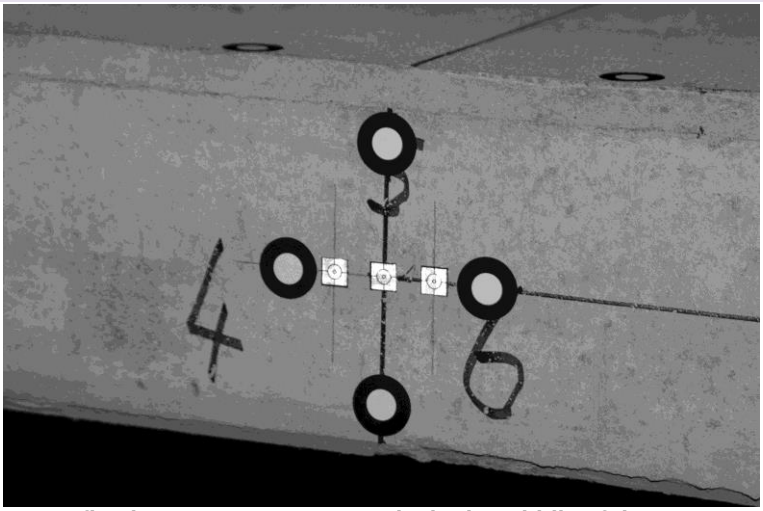

Figure 2. Reflective tape targets 4, 5 and 6 in the middle of the concrete plate

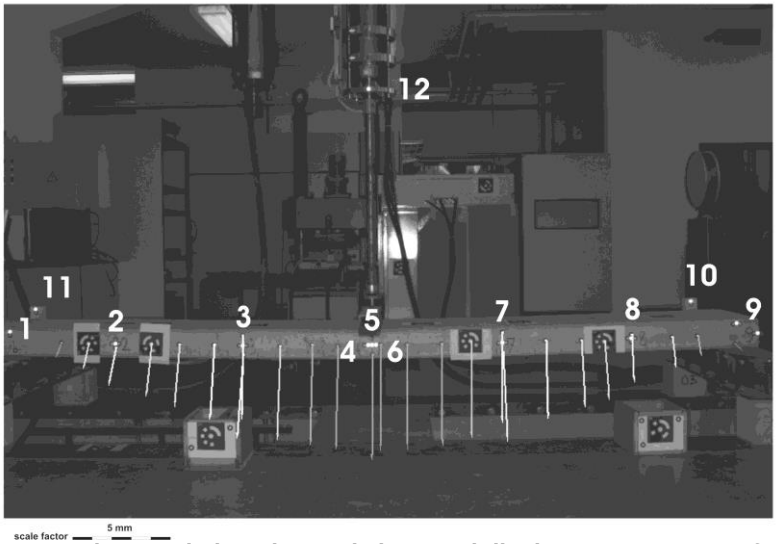

Figure 3. Reference points, coded marks, scale bars and displacement vectors of a concrete plate

Test configuration

The deflections of the plate depend on the geometrical and material characteristics of the test sample. The expected vertical displacement was analytically determined using the appropriate static model and Eurocode 2 Standard [1].

Geometrical characteristics:
Calculated static length: *L = 3750 mm*
Width: *b = 500 mm*

Height: ***h = 150 mm***
Effective depth of a cross-section: ***d = 120 mm***
Cross sectional area of tensile reinforcement: A_{s1}^{+} = 7.70 cm^2 (5 ϕ14 mm)
A_{s2}^{+} = 0.724 cm^2 (3x3 ϕ 3.2 mm)
Cross sectional area of compressive reinforcement: A_s^{-} = 3.93 cm^2 (5 ϕ 10 mm)
Material characteristics:
Concrete:

Strength class: *C 30/37*
Mean tensile strength: f_{ctm} *= 2.9 MPa*
Modulus of elasticity: $E_{cm}=32\cdot10^6$ *kN/m*^{2}
Reinforcement:

Strength class: *S 400 (A_{s1}^+, A_s^-) , S 1680 (A_{s2}^+)*
Characteristic yield strength: f_{yk} = *400 MPa*
Design value of modulus of elasticity: $E_s=200\cdot10^6$ *kN/m²*

Analytical results

While the well-known analytical methods can be used for calculation of non-cracked cross-sectional displacements, some problems are encountered for cracked cross-sections where cracks occur in the tensile area due to the low tensile strength of the concrete. This results in a reduction of the second moment of the concrete section area and consequently in an increased deflection. As it is difficult to exactly determine the location as well as the size of the cracks, they are usually modelled using different national codes. Eurocode 2 [1] is most frequently applied in Europe and therefore considered in our analysis.

According to the above characteristics, the second moment of the area of the un-cracked cross-section is $I_y^{(I)}=15345.478\ cm^4$. The predicted vertical displacement was calculated using the applicable static design with the vertical force in the middle of the span, as shown in figure. 4.

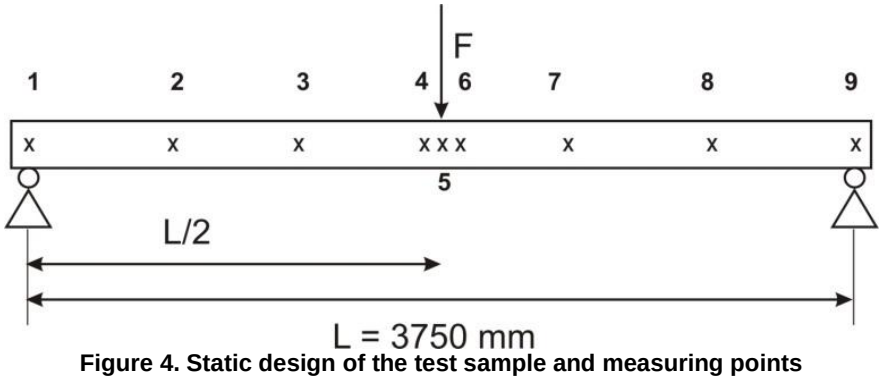

Figure 4. Static design of the test sample and measuring points

The bending moment forming the first crack in the tensile concrete section ($M_y^{(I)}$) is calculated in the form of:

$$M_y^{(I)} = f_{ctm} \cdot \frac{2 \cdot I_y^{(I)}}{h} = 0.29 \cdot \frac{2 \cdot 15345.478}{15} = 593.36\ kNcm = 5.9336\ kNm \tag{6}$$

The maximal vertical displacement (w_{inst}) is the sum of the bending moment (M_{y0}) for the un-cracked cross-section ($M_{y0} \le M_y^{(I)}$), the shear force due to the actual load on the structure (V_{z0}), the shear force due to the virtual load on the structure ($\overline{V}_{z1}(x)$) and the axial force (N_0) contribution in the form of:

$$w_{init} = w_{init,M} + w_{init,V} + w_{init,N} =$$

$$= \int_S \frac{M_{y0}(x) \cdot \overline{M}_{y1}(x)}{E_{cm} \cdot I_y^{(I)}} dx + \int_S \frac{V_{z0}(x) \cdot \overline{V}_{z1}(x)}{G_{cm} \cdot A_{cs}} dx + \int_S \frac{N_0(x) \cdot \overline{N}_1(x)}{E_{cm} \cdot A_c} dx \tag{7}$$

where:

$\overline{N_1}(x)$ = axial force due to virtual point load

$N_0(x)$ = axial force due to actual load on the structure

A_c = cross sectional area of concrete

M_{y0} (x) = bending moment due to actual load on the structure

$\overline{M}_{y1}(x)$ = bending moment due to virtual point load

For the given static design (Fig 4.) Eq. (7) results in:

$$w_{init} = \frac{F \cdot L^3}{48 \cdot E_{cm} \cdot I_{yI}} + \frac{1.2 \cdot F \cdot L}{4 \cdot G_{cm} \cdot A_{cs}} \tag{8}$$

where $G_{cm} = \frac{E_{cm}}{2 \cdot (1 + \nu_c)}$, $A_{cs} = \frac{A_c}{1.2}$, F = force acting on the middle of the span (see figure 4) and ν_c Poisson's ratio.

For the cracked cross-section ($M_{y0} > M_y^{(I)}$) the maximal vertical displacement (w_{inst}) is calculated as:

$$w_{init} = w_{init,M} + w_{init,V} + w_{init,N} =$$
$$= \int_S \frac{M_{y0}(x) \cdot M_{y1}(x)}{E_{cm} \cdot I_{y,eff}^{(II)}} dx + \int_S \frac{V_{z0}(x) \cdot V_{z1}(x)}{G_{cm} \cdot A_{cs,eff}^{(II)}} dx + \int_S \frac{N_0(x) \cdot N_1(x)}{E_{cm} \cdot A_{c,eff}^{(II)}} dx \quad (9)$$

where the effective second moment of area of the cracked cross-section ($I_{y,eff}^{(II)}$) is determined according to Eurocode 2 [1] in the form of:

$$I_{y,eff}^{(II)} = \xi \cdot \mathrm{I}_{\mathrm{y}}^{(\mathrm{II})} + (1-\xi) \cdot \mathrm{I}_{\mathrm{y}}^{(\mathrm{I})}$$
$$\xi = 1 - \beta_1 \cdot \beta_2 \cdot \left(\frac{\mathrm{M_{yI}}}{\mathrm{M_{y0,max}}}\right)^2 \quad (10)$$
$$M_{y0,\max} = \frac{F \cdot L}{4}; \quad \beta_1 = 1.0, \ \beta_2 = 1.0$$

The value of $I_y^{(II)}$, representing the second moment of area of the cracked cross-section, is calculated according to the neutral axis position (x_{II}) using the scheme shown in Fig. 5. The neutral axis position (x_{II}) is calculated taking into account the un-cracked compressive concrete cross-section, tensile and compressive reinforcement, as follows:

$$\frac{b \cdot x_{II}^2}{4} + (n-1) \cdot A_s^- \cdot (x_{II} - a_3) - n \cdot A_{s1}^+ \cdot (h - a_1 - x_{II}) - n \cdot A_{s2}^+ \cdot (h - a_2 - x_{II}) = 0$$
$$x_{II} = 4.948\,cm$$
$$I_y^{(II)} = \frac{b \cdot x_{II}^3}{3} + (n-1) \cdot A_s^- \cdot (x_{II} - a_3)^2 + \quad (11)$$
$$+ n \cdot A_{s1}^+ \cdot (h - a_1 - x_{II})^2 + n \cdot A_{s2}^+ \cdot (h - a_2 - x_{II})^2 = 4757.344\,cm^4$$
$$n = \frac{E_S}{E_{cm}}$$

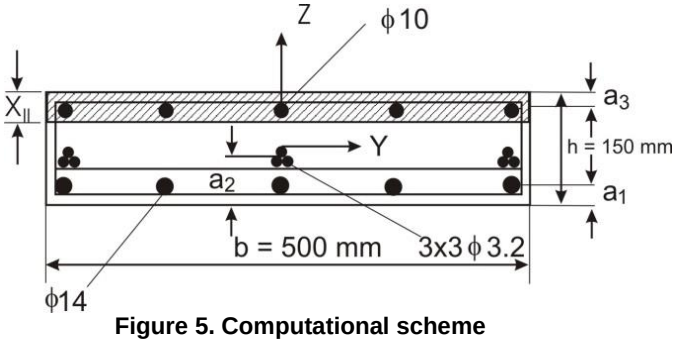

Figure 5. Computational scheme

Comparison of results

A comparison of the measurements of vertical displacements of the whole concrete plate was made. A comparison between the analytical and the measured geodetic, photogrammetric and length sensor vertical displacements were made. Figure 6 shows the vertical displacements for point 5 in the middle of the concrete plate. (Only point 5 was monitored with all three methods.) In practice, there is an unwritten rule that the ratio between the calculated and the measured value should not be less than 75 %. When omitting the first two epochs, the mean ratio between the calculated and the measured values was 88.5 %.

The geodetic and photogrammetric results were comparable (some tenths of mm) for Point 5 (figure 6). It can be seen that the surveyed vertical displacement was always smaller than the calculated values. There is a small deviation in the first two epochs because the local contact surface under the pressure length transducer was undefined.

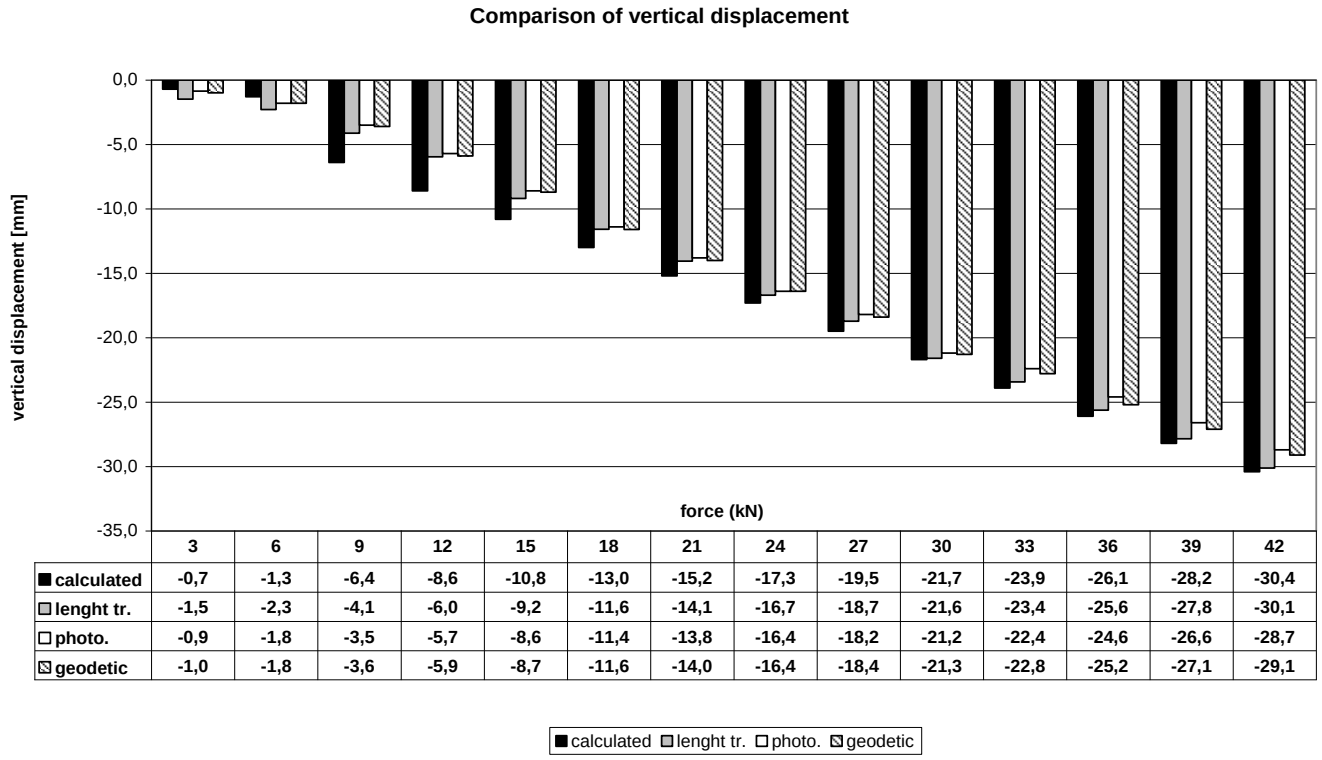

	3	6	9	12	15	18	21	24	27	30	33	36	39	42
calculated	-0,7	-1,3	-6,4	-8,6	-10,8	-13,0	-15,2	-17,3	-19,5	-21,7	-23,9	-26,1	-28,2	-30,4
lenght tr.	-1,5	-2,3	-4,1	-6,0	-9,2	-11,6	-14,1	-16,7	-18,7	-21,6	-23,4	-25,6	-27,8	-30,1
photo.	-0,9	-1,8	-3,5	-5,7	-8,6	-11,4	-13,8	-16,4	-18,2	-21,2	-22,4	-24,6	-26,6	-28,7
geodetic	-1,0	-1,8	-3,6	-5,9	-8,7	-11,6	-14,0	-16,4	-18,4	-21,3	-22,8	-25,2	-27,1	-29,1

Figure 6. Comparison of the vertical displacements in point 5

Mathematical approximation

For every load case (3 kN, 9 kN, 15 kN, …) polynomials of degree 3 through the monitoring points were fitted with the Mathematica 5.0 software. The polynomials of degree 3 are of the form

$$p_i(x) = a_i + b_i\, x + c_i\, x^2 + d_i\, x^3 \tag{12}$$

for i = 1, 2, … n, where n is the number of observed control points on the concrete plate (7 points) and x is the length of the concrete plate. Fig. 7 shows the magnitude of vertical displacements at the different loads. The calculated polynomials are also given in Table 2. (For the sake of better presentation, the units for x and y axis are metres [m] and millimetres [mm], respectively.) Note that the $p(x)$ represents the vertical displacement of the plate at point x caused by the force $\vec{F}$.

Additionally, the polynomials were calculated for the deformations at seven monitoring points versus load. This time, the x and y represents the load (in kN) and the vertical displacement (in mm) caused by that force at the given monitoring points.

Table 2. Polynomials through points 1-9 for different loads

Load	$p_i(x)$ in mm, x in m
	polynomial
3 kN	$0.164286 - 1.00571\,x - 0.237714\,x^2 - 1.54405 \cdot 10^{-16}\,x^3$
9 kN	$0.233333 - 3.79175\,x - 1.00876\,x^2 - 0.0113778\,x^3$
15 kN	$0.430952 - 8.58159\,x - 2.0541\,x^2 - 0.0455111\,x^3$
21 kN	$0.883333 - 14.1352\,x - 3.3981\,x^2 - 0.0682667\,x^3$
27 kN	$1.70952 - 19.066\,x - 4.59886\,x^2 - 0.0910222\,x^3$
33 kN	$2.42857 - 24.5156\,x - 6.15924\,x^2 - 0.0568889\,x^3$
39 kN	$3.33333 - 29.4546\,x - 7.33562\,x^2 - 0.0910222\,x^3$

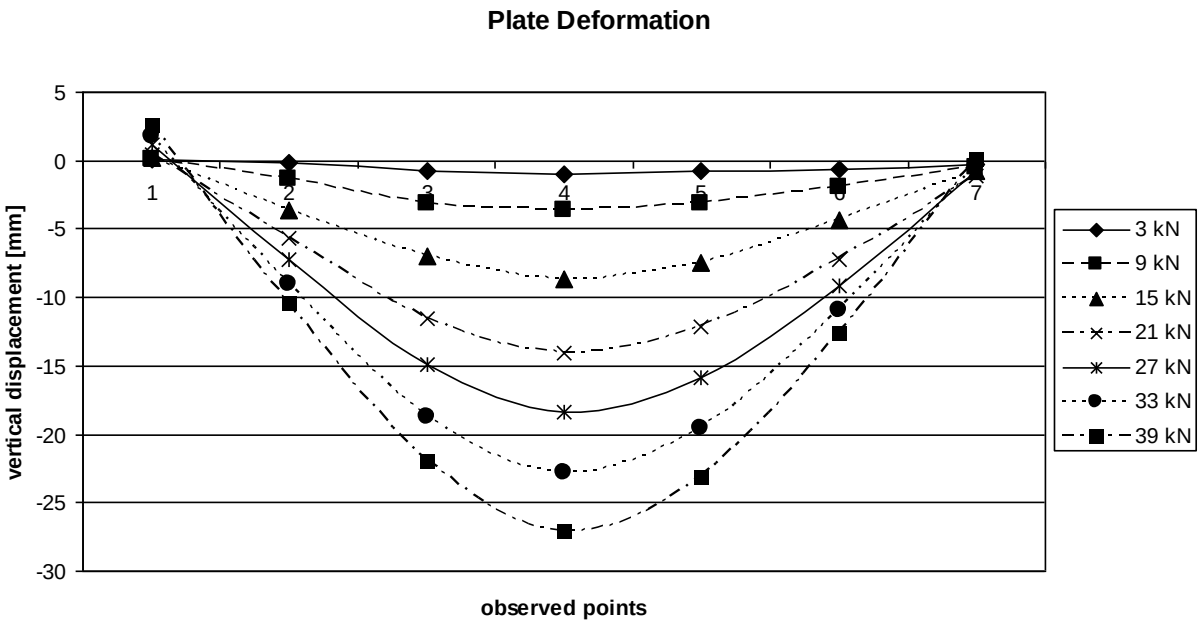

Figure 7. Graphs of fitted polynomials for seven load cases (3 kN,…, 39 kN)

This shows the behaviour of the concrete plate at intermediate forces (e.g. 6 kN, 12 kN, 18 kN, …). It is important to mention that these functions are very useful, because we don't need to measure the displacements separately for every single force. The fitted polynomials for the individual points for forces 3 kN, 9 kN, 15 kN, 21 kN, 27 kN, 33 kN, 39 kN are given in Table 3. The results show that in future experiments there is no need to fit the predicted deformations with a third degree polynomial. It would be sufficient to model the predicted deformations by a linear or, possibly, quadratic function as is evident in Fig. 8.

Table 3: Vertical deformation (y) of individual points versus applied load (x) (3 kN, 9 kN,…)

Point	Vertical Deformation (*y* in mm) =
1	$-0.260119 - 0.0581019\,x - 0.00403439\,x^2 - 0.0000257202\,x^3$
2	$0.548661 - 0.195486\,x + 0.0067295\,x^2 - 0.000115741\,x^3$
3	$0.294792 - 0.262583\,x + 0.0193948\,x^2 - 0.000295782\,x^3$
5	$0.399405 - 0.322288\,x + 0.0237434\,x^2 - 0.000360082\,x^3$
7	$0.466964 - 0.297222\,x + 0.0198743\,x^2 - 0.000308642\,x^3$
8	$0.12247 - 0.161095\,x + 0.0126819\,x^2 - 0.000218621\,x^3$
9	$-0.109375 - 0.0515377\,x - 0.00014881\,x^2 - 0.0000385802\,x^3$

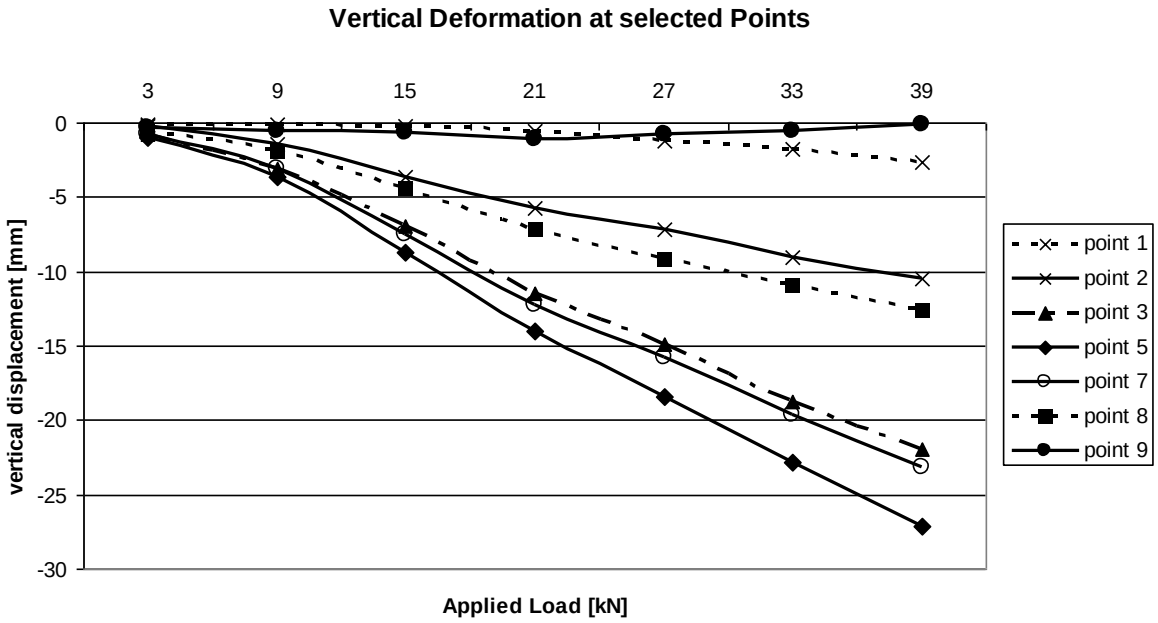

Figure 8. Graphs of vertical deformations for all seven monitoring points versus applied load

Using the fitted curves the displacements at 6 kN, 12 kN, 18 kN … were calculated for every monitoring point. The values were then compared with the actual measurements at these loads. The calculated and measured values for point 5, where the displacements were largest, as well as their differences, are shown in Table 4. The mean value of the deviations is 5.7 %. The deviation is at 6 kN, because of very small vertical displacement of -1.8 mm largest. If we omit this force (6 kN), the mean deviation is better (3.0 %).

Table 4: Comparison of calculated and measured values for point 5

Load [kN]	Vertical Displacement [mm]		Deviation [%] 100-(meas/calc · 100)
	calculated	measured	
6	-2.3	-1.8	+ 21.7
12	-6.3	-5.9	+ 6.3
18	-11.0	-11.6	- 5.2
24	-16.0	-16.4	- 2.4
30	-20.9	-21.3	- 1.9
36	-25.2	-25.2	0.0
42	-28.4	-29.1	- 2.4
		mean value	5.7

The differences between the calculated and the measured values for the other points are shown in Table 5. The points 1 and 9 were omitted from the analysis since the beam was not supported perfectly rigid at these points and the measured vertical displacements were not accurate at those points (in theory they should be 0.0 mm). The comparison for a load of 24 kN can be seen in figure 9.

Table 5. Mean differences (in %) between calculated and measured displacements at selected points

Point	Difference [%]
2	+ 1.9
3	+ 4.6
5	+ 5.7
7	+ 5.0
8	+ 2.2
mean value	+ 3.9

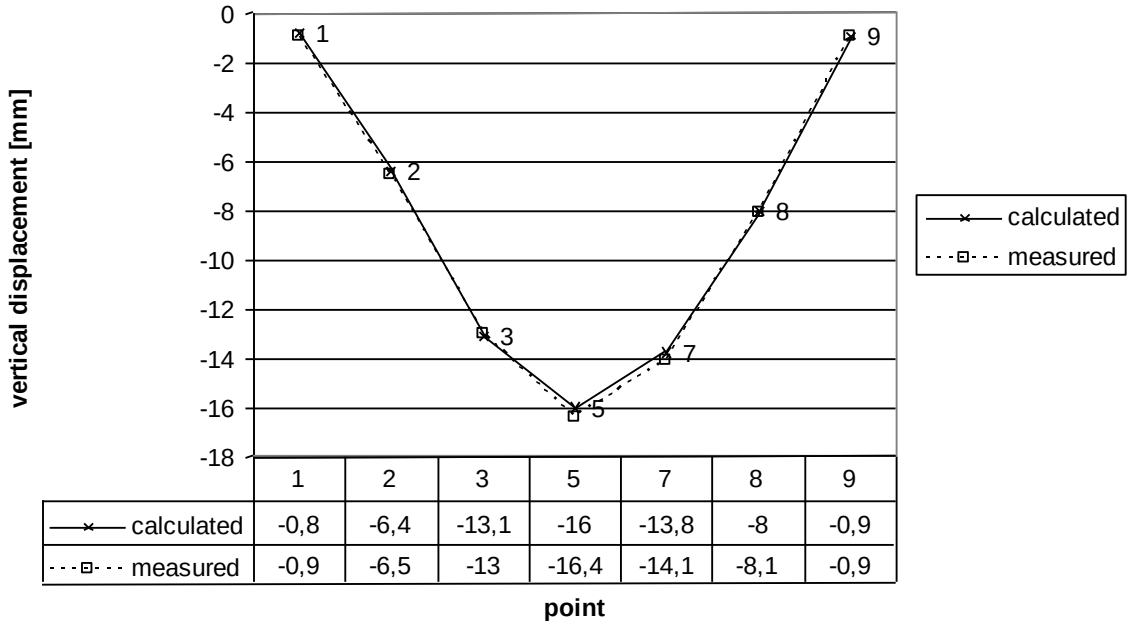

	1	2	3	5	7	8	9
calculated	-0,8	-6,4	-13,1	-16	-13,8	-8	-0,9
measured	-0,9	-6,5	-13	-16,4	-14,1	-8,1	-0,9

Figure 9. Comparison of calculated and measured displacements for a concrete plate of 3.75 m length at a load of 24 kN

Conclusions

Measurement technologies have developed in the field of displacement and deformation measurements. Not long ago, tacheometers and levelling instruments were the chosen surveying methods and different length transducers as physical methods. The development also reached the field of bridge construction where the deformation under load has to be established before commissioning. Since bridges traverse narrow valleys, gorges and rivers, the set-up of instruments is often impossible and the use of the levelling method troublesome because of pre-stressed forms.

Taking all these problems into account, we are searching for solutions to accomplish the measurements and lower the numbers of measurements. As an alternative measurement method, photogrammetry was used. It proved very useful since no control points are needed in the field; more important is the large number of images obtained from different camera stations. For the purpose of monitoring, trigonometric heighting was used which is irreplaceable for such measurements. The results are comparable within the allowed limits. To control the comparison of measured values, which are affected by external factors (temperature, distance, incline of measurements…), theoretical values were calculated using Eurocode 2. The measured values were entirely compatible.

Our largest contribution to science and development in the field of result evaluation and presentation is the mathematical analysis in the form of fitted polynomials. The achieved results offer a quicker assessment of the measurement performance, provide intermediate values which are not required or are impossible to measure, and give an estimate of the displacements. The values for intermediate points are also obtained, i.e. between two measurement points in horizontal direction. In future, it is reasonable to use such an procedures on larger and more demanding constructions, where it is not possible to get the required number of measurements, so that the whole procedure of load testing is accelerated and the associated costs are reduced.

References

[1]. CEN, Eurocode 2. (2002) Design of concrete structures – Part 1: General rules and rules for buildingsю

[2]. Ataei, S. et al., Sensor fusion of a railway bridge load test using neural networks (2005) Expert Systems with Applications. 29. Pp. 678-683.

[3]. Dörstel, C., Jacobsen K., Stallmann D. DMC – Photogammetric accuracy – Calibration aspects and generation of sythetic DMC images (2003) Proc., Optical 3D Measurements Symposium, Zurich, Pp. 74-82.

[4]. Albert, J., Maas H. G., Schade, A., Schwarz, W. Pilot studies on photogrammetric bridge deformation measurement, IAG Berlin, (2002) Proc., 2nd Symposium on Geodesy for Geotechnical and Structural Engineering, Vienna University of Technology, Institute of Geodesy and Geophysics, Berlin, Germany, May 21-24, Pp. 133-140.

[5]. Gordon, S. et. al. Measurement of Structural Deformation using Terrestrial Laser Scanners (2004) 1st FIG International Symposium on Engineering Surveys for Construction Works and Structural Engineering, Nothingham, UK, 28 June – 1 July, Pp. 876-884.

[6]. Vodopivec, F. Trigonometric heights. Department of Civil Engineering and Department of Geodesy FAGG (1985) University of Ljubljana, Pp. 57-68.

[7]. Moser, A. Engineering Geodesy, Basics (2000) 3rd ed, Wichmann, Heidelberg, Germany.

[8]. Gorjup, Z. The photogrammetry and calculation of accuracy (2001) University in Ljubljana, Faculty of Civil Engineering and Geodesy, Ljubljana, Pp. 8-17.

[9]. Maas, H., G., Hampel, U. Photogrammetric Techniques in Civil Engineering Material Testing and Structure Monitoring (2006) Photogrammetric Engineering & Remote Sensing. 72 (1). Pp. 1-7.

[10]. Platonova M. A., Vatin N. I., Nemova D. V., Matoshkina S. A., Iotti D., Togo I. The influence of the airproof composition on the thermo technical characteristics of the enclosing structures (2014) Construction of Unique Buildings and Structures, 4 (19). Pp. 83-95.

[11]. Kishinevskaya, Ye. V. Vatin, N. I. Kuznetsov, V. D. *Perspektivy primeneniya nanobetona v monolitnykh bolsheproletnykh rebristykh perekrytiyakh s postnapryazheniyem* [Application of nanoconcrete in post-stressed monolithic span ribbed slabs], Magazine of Civil Engineering. 2 (2009), Pp. 54-58.

[12]. Gorshkov A. S., Vatin N. I. Properties of the wall structures made of autoclaved cellular concrete products on the polyurethane foam adhesive (2013) Magazine of Civil Engineering. 5 (40). Pp. 5-19.

[13]. Vatin N. I., Pestryakov I. I., Kiski S. S., Teplova Z. S. Influence of the geometrical values of hollowness on the physicotechnical characteristics of the concrete vibropressed wall stones (2014) Applied Mechanics and Materials, Vols. 584-586, Pp. 1381-1387.

[14]. Grinfeldi G. I., Gorshkov A. S., Vatin N. I. Tests results strength and thermophysical properties of aerated concrete block wall samples with the use of polyurethane adhesive. Advanced Materials Research, Vols. 941-944, (2014), Pp. 786-799.

[15]. Gouverneur, D., Caspeele, R., Taerwe, L. Experimental investigation of the load– displacement behaviour under catenary action in a restrained reinforced concrete slab strip (2013) Engineering Structures, Vol. 49 , Pp. 1007-1016.

[16]. Garden, H.N., Hollaway, L.C. An experimental study of the failure modes of reinforced concrete beams strengthened with prestressed carbon composite plates (1998) Composites Part B: Engineering, Vol. 29(4), Pp. 411-424

[17]. Avril, S., Vautrin, A., Hamelin, P., Surrel, Y. A multi-scale approach for crack width prediction in reinforced-concrete beams repaired with composites (2005) Composites Science and Technology, Vol. 65(3–4), Pp. 445-453.

[18]. Biscaia , H., Chastre, C., Silva , S. A smeared crack analysis of reinforced concrete T-beams strengthened with GFRP composites (2013) Engineering Structures, Vol. 56, Pp. 1346-1361.

[19]. Hu, H.S., Nie, J. G., Eatherton, M. R. Deformation capacity of concrete-filled steel plate composite shear walls {2014) Journal of Constructional Steel Research, Vol. 103, Pp. 148-158.

[20]. Subedi, N. K., Baglin, P. S. Ultimate load analysis of plate reinforced concrete beams (2001) Engineering Structures, Vol. 23(9), Pp. 1068-1079.

Взаимосвязи между деформациями и нагрузками для железобетонных пластин

Б. Ковачич[1], **Р. Камник**[2]

Университет Марибора, Словения, Сметанова ул. 17, SI – 2000 Марибор.

Информация о статье	**История**	**Ключевые слова**
УДК 69 Научная статья	Подана в редакцию 22 декабря 2014 Принята 28 декабря 2014	измерение смещений, электронный тахеометр, фотограмметрии, длина датчик давления на гидравлическом цилиндре, железобетонная плита.

АННОТАЦИЯ

В настоящее время методы измерения деформаций конструкций хорошо известны. Разнообразие оборудования различной точности и мощности доступно. В этой статье мы представляем комбинированный метод тахеометрических и фотограмметрических измерений и смещений, измеренных длины датчика давления. В нашей лаборатории, загрузка предварительно напряженных бетонных плит производилась с шагом 3 кН. Программа Mathematica 5.0 была использована для расчета интерполяции многочленами. Все результаты проанализированы в соответствии с расчетными значениями (с использованием Еврокода 2) с помощью интерполяционных многочленов. Результаты показывают, что в будущем нам не придется использовать так много фаз нагрузки, потому что промежуточные перемещения могут быть вычислены из полученных уравнений, и смещения при различных нагрузках можно предсказать.

[1] *Контактный автор:*
bostjan.kovacic@uni-mb.si (Ковачич Боштьян, к.т.н., профессор)
[2] rok.kamnik@um.si (Камник Рок, к.т.н., Associate Professor)

Литература

[1]. CEN, Eurocode 2. (2002) Design of concrete structures – Part 1: General rules and rules for buildingsю

[2]. Ataei, S. et al., Sensor fusion of a railway bridge load test using neural networks (2005) Expert Systems with Applications. 29. Pp. 678-683.

[3]. Dörstel, C., Jacobsen K., Stallmann D. DMC – Photogammetric accuracy – Calibration aspects and generation of sythetic DMC images (2003) Proc., Optical 3D Measurements Symposium, Zurich, Pp. 74-82.

[4]. Albert, J., Maas H. G., Schade, A., Schwarz, W. Pilot studies on photogrammetric bridge deformation measurement, IAG Berlin, (2002) Proc., 2nd Symposium on Geodesy for Geotechnical and Structural Engineering, Vienna University of Technology, Institute of Geodesy and Geophysics, Berlin, Germany, May 21-24, Pp. 133-140.

[5]. Gordon, S. et. al. Measurement of Structural Deformation using Terrestrial Laser Scanners (2004) 1st FIG International Symposium on Engineering Surveys for Construction Works and Structural Engineering, Nothingham, UK, 28 June – 1 July, Pp. 876-884.

[6]. Vodopivec, F. Trigonometric heights. Department of Civil Engineering and Department of Geodesy FAGG (1985) University of Ljubljana, Pp. 57-68.

[7]. Moser, A. Engineering Geodesy, Basics (2000) 3rd ed, Wichmann, Heidelberg, Germany.

[8]. Gorjup, Z. The photogrammetry and calculation of accuracy (2001) University in Ljubljana, Faculty of Civil Engineering and Geodesy, Ljubljana, Pp. 8-17.

[9]. Maas, H., G., Hampel, U. Photogrammetric Techniques in Civil Engineering Material Testing and Structure Monitoring (2006) Photogrammetric Engineering & Remote Sensing. 72 (1). Pp. 1-7.

[10]. Platonova M. A., Vatin N. I., Nemova D. V., Matoshkina S. A., Iotti D., Togo I. The influence of the airproof composition on the thermo technical characteristics of the enclosing structures (2014) Construction of Unique Buildings and Structures, 4 (19). Pp. 83-95.

[11]. Кишиневская Е.В., Ватин Н.И., Кузнецов В.Д. Перспективы применения нанобетона в монолитных большепролетных ребристых перекрытиях с постнапряжением // Инженерно-строительный журнал. 2009. №2. С. 54-58.

[12]. Gorshkov A. S., Vatin N. I. Properties of the wall structures made of autoclaved cellular concrete products on the polyurethane foam adhesive (2013) Magazine of Civil Engineering. 5 (40). Pp. 5-19.

[13]. Vatin N. I., Pestryakov I. I., Kiski S. S., Teplova Z. S. Influence of the geometrical values of hollowness on the physicotechnical characteristics of the concrete vibropressed wall stones (2014) Applied Mechanics and Materials, Vols. 584-586, Pp. 1381-1387.

[14]. Grinfeldi G. I., Gorshkov A. S., Vatin N. I. Tests results strength and thermophysical properties of aerated concrete block wall samples with the use of polyurethane adhesive. Advanced Materials Research, Vols. 941-944, (2014), Pp. 786-799.

[15]. Gouverneur, D., Caspeele, R., Taerwe, L. Experimental investigation of the load– displacement behaviour under catenary action in a restrained reinforced concrete slab strip (2013) Engineering Structures, Vol. 49 , Pp. 1007-1016.

[16]. Garden, H.N., Hollaway, L.C. An experimental study of the failure modes of reinforced concrete beams strengthened with prestressed carbon composite plates (1998) Composites Part B: Engineering, Vol. 29(4), Pp. 411-424

[17]. Avril, S., Vautrin, A., Hamelin, P., Surrel, Y. A multi-scale approach for crack width prediction in reinforced-concrete beams repaired with composites (2005) Composites Science and Technology, Vol. 65(3–4), Pp. 445-453.

[18]. Biscaia , H., Chastre, C., Silva , S. A smeared crack analysis of reinforced concrete T-beams strengthened with GFRP composites (2013) Engineering Structures, Vol. 56, Pp. 1346-1361.

[19]. Hu, H.S., Nie, J. G., Eatherton, M. R. Deformation capacity of concrete-filled steel plate composite shear walls {2014) Journal of Constructional Steel Research, Vol. 103, Pp. 148-158.

[20]. Subedi, N. K., Baglin, P. S. Ultimate load analysis of plate reinforced concrete beams (2001) Engineering Structures, Vol. 23(9), Pp. 1068-1079.